HYDRODYNAMIC MODELLING OF SEMI-DISPLACEMENT MULTI-HULL VESSELS

Giuseppina Colicchio*, Andrea Colagrossi*, Marilena Greco*, Claudio Lugni*, Odd Magnus Faltinsen**
*Italian Ship Model Basin (INSEAN)
Via di Vallerano 139, 00128 Roma, Italy
**Centre for Ships and Ocean Structures (CeSOS)
Trondheim, Norway

ABSTRACT

Both experimental and numerical tools are used to investigate the steady flow field around a trimaran vessel. The experimental measurements are used to state the reliability of two numerical algorithms: a fully nonlinear 2D+t potential flow solver and a linear 3D-RPM numerical model. Then, the two solvers have been used to study the physical features highlighted by the experiments, more in particular to identify the interference and linear and nonlinear hydrodynamic interaction among the hulls and behind the transom stern

INTRODUCTION

Trying to increase the speed of marine vehicles, designers have introduced new hull forms and configurations as with the trimarans.
The use of multi-hulls requires a careful analysis of stability and manoeuvrability.
Moreover, designers demand to be able to estimate the interaction among the hulls of the ship and to forecast the dynamics of the whole arrangement in different sea conditions and ship speeds.
The present paper describes part of a study that aims to understand the physics of slender hull forms and the phenomena of interaction when several hulls are coupled in the same ship.
Using the same hull shape, a systematic study of a mono-hull and a catamaran in calm water and head sea [1], and a trimaran in calm water [2] , has been carried out for a large range of Froude numbers.
The investigation has been performed with both the numerical and experimental tools of analysis.
In this context, Doctors [3] showed that, for the multihulls, the mathematical models often fail to predict the fluid dynamic field.
Therefore the experiments are used here both to identify the physical features involved and to help the validation of the numerical solvers in the different conditions.
So that, the aspects highlighted in the experiments can be further studied with the most suitable numerical method.
More in particular, here a trimaran configuration will be analyzed with a large central hull and smaller outriggers.
The numerical tools will help to understand the effect of the interference among the wave patterns generated by the individual hulls and the linear and nonlinear hydrodynamic interactions.
In the following it will be shown that the nonlinear effects are more evident for the main hull than for the side hull, even though this moves to a relatively higher Froude number.
Moreover it will be also evident that close to the transom region the flow is highly three-dimensional and that any solver that disregards this characteristics is due to fail to capture the correct wave pattern and may only give a qualitative information on the interference and interaction among the wave systems.

1. DESCRIPTION OF THE TRIMARAN GEOMETRY

The geometry of the trimaran is described in Table 1.

Geometric characteristics	
Scale factor	6.25
L_{pp} (m)	25
B_{WL} (m)	7.156
D (m)	1.740
W_y (m)	3
Volume (m^3)	47.962
LCB (m)	9.92
KG (m)	3
GM_T (m)	0.915
GM_L (m)	37.13
k_{yy}	$0.26*L_{pp}$

Table 1: *Geometric characteristics of the Trimaran vessel.*

The side hulls have the same geometry as the central hull and their dimensions are scaled according to the geometric ratios normally used for this kind of multihull configuration. A sketch of the cross-sections for the three hulls is given in Fig. 1. The distance W_y between the main hull and the outriggers has been evaluated by means of a preliminary static calculation of the transversal stability.
A detailed sketch of the longitudinal position of the wave probes along the vessel is reproduced in Fig. 2.

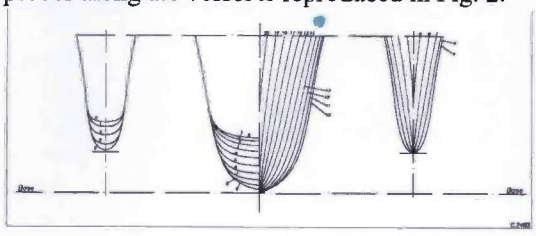

Fig. 1: *Cross sections of the trimaran.*

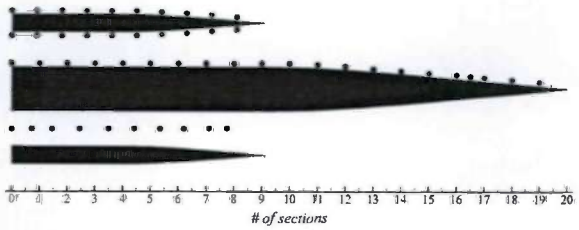

Fig. 2: *Sketch of the wave probe system for the measurements of the hull profiles. The longitudinal position of the wave probes is indicated in terms of the section numbers.*

2. EXPERIMENTAL SET-UP

The experiments were performed in the INSEAN basin No. 2. It is 220 m long, 9 m large and 3.6 m deep. The model was equipped with the classical test rig used at INSEAN for the seakeeping tests. A gimble allows only the pitch rotation around the COG position and restrains the other rotational degrees of freedom. A dedicated mechanical system leaves the heave motion free, while restraining surge and sway.

To stimulate the turbulence in calm-water conditions, strips of sand were used both on the main hull and on the lateral ones.

A capacitance wave probe system, composed by 51 transducers arranged as in the sketch of Fig. 2, was used to record: 1) the wave profile of the main hull, 2) the external and internal ones at the outriggers and 3) the longitudinal cut along the meanline between the central hull and the outriggers. The transducers used for the hull profile measurements, were mounted parallel to the longitudinal sections and tangentially to the hull surface at a distance of few millimeters. In this preliminary analysis, the experimental data were not corrected by including the inclination of the wires with respect the vertical line (maximum angle: 6-8 degrees).

A detailed investigation of the wave elevation behind the transom stern has been performed in calm water.

For this purpose, two different set-up were considered: a transversal rake to measure the 3D wave pattern behind the stern, and two finger probes to determine the longitudinal cut in correspondence of the centerlines of the main and lateral hulls.

An array of 20 capacitance wave probes was placed parallel to the transom stern of the central hull. Assuming the symmetry of the wave field with respect to the centerline of the trimaran, only the left half-plane was considered: the first wave probe was positioned at a distance of 8 mm from the centerline while the distance between two successive transducers was fixed to 3 cm.

A step-by-step motor was used to change the longitudinal position of the array of transducers, so that several longitudinal positions were investigated for each run. The longitudinal displacement dx enforced through the motor was not constant but varied depending on the distance from the transom stern: a minimum dx = 1.25 cm was used in the hull hollow region, dx=2.5 cm in the area of the rooster tail, and dx=5 cm in the far field region.

In the region with smallest dx, the same linear guide system used for the rake has been adopted to change the longitudinal position of the finger probes.

Particular care has been taken in performing a dedicated error analysis of the wave probes close to the hulls. On this purpose, in the calm-water tests each run was repeated between 10 and 20 times. The error analysis did not include the bias error, but just the precision one.

3. NUMERICAL FORMULATION

The problem is analyzed numerically by means of two different solvers: 1) a 3D linear Rankine Panel Method and 2) a fully non linear 2D+t theory with a BEM solver. In the following, the features of the two methods are briefly outlined.

3.1. 3D linear solution

The flow field induced by a ship advancing at constant forward speed U in calm water is solved using a linear potential flow theory.

A velocity potential is introduced and the hypothesis of a divergent free velocity leads to the Laplace equation.

This equation is coupled to the body and free-surface boundary conditions. In particular, the free-surface boundary conditions are transferred on the undisturbed free surface using a Double-Model (DM) linearization, that is the double-body flow is adopted as base flow (see *i.e.*[5]).

Once known the velocity potential, the kinematic free surface condition furnishes the steady wave pattern.

Numerically, the velocity potential is expressed in terms of discrete source distributions on the body H and on the free surface W.

In particular, a lower order Rankine Panel Method has been applied (*RPM*, [6]). The collocation points on H and on W are placed at the centers of the panels, but the ones on the free surface are rigidly shifted one panel upstream in order to enforce numerically the radiation condition (see *i.e.*[7]).

During the experiments the transom stern was observed always dry. This is consistent with the findings of Doctors [8], i.e. the local Froude number referred to the draft, Fr_T, is higher than 2.09.

In the literature, different numerical techniques have been introduced to be able to model such condition within a 3D potential theory (see *i.e.*[9]).

Most of these methods present the drawbacks of weakly robust mathematical formulations and of a not straightforward extension to multi-hull geometries.

Here a *false body* is added to the original hull to enforce the flow to detach tangentially from the body and to smoothly reconcile it with the free surface.

The shape of the *false body* is defined by three different curves: 1) the transom section, 2) a parabolic profile in the xz plane with a curvature equal to $(2Fr^2)^{-1}$, and 3)

polynomial curve in the *xy* plane that reconnects the other two.
As an alternative, the second curve described above has been substituted by the experimental cut in the midline of each hull.
In the simulations the dummy portion of the hull is not taken into account when computing the loads.
The results obtained with the different shapes of the false body will be discussed in the next section.

3.2. 2D+t theory

Assuming that the velocity variation along the longitudinal axis is small when compared with the transversal variations, the 2D+t theory neglects it and considers u constant all over the fluid field and equal to U. This simplification allows to analyze the 3D problem of a ship advancing with constant forwad speed by means of a 2D unsteady problem. Practically the evolution of the flow field is studied in a fixed plane parallel to the ship cross-sections. In this plane the flow is initially perturbed by the appearance of the body, as the hull crosses the plane.
The deformation of the free surface is continuously enforced by the deformation of the cross section of the hull.
This theory applies the hypotheses of inviscid and irrotational flow, so that a velocity potential ϕ can be introduced and the governing equation is the *2D* Laplace equation, with the impermeability boundary condition on the hulls and the kinematic and dynamic conditions on the free surface.
This 2D unsteady problem is solved numerically through a Mixed Eulerian Lagrangian method.
The kinematic problem is solved applying the Green's second identity in its integral representation of the velocity potential.
A Boundary Element Method (BEM) is used for its discretization, linear shape functions represent the geometry and the boundary data.
The time evolution is discretized using a 4^{th} order Runge-Kutta method.
The discretization of the free surface is subject to grid refinement and regridding to follow its high deformations.
The BEM can capture the formation of very thin jets and of plunging waves. But it is not able to follow them when they break up.
To avoid the problem, the jets are suitably cut, according to the method suggested in [4]. The unphysical reflection of the wave from the numerical far field boundaries is avoided by using both a damping layer and a stretching of the panels.
It has been shown that the 2D+t theory is suitable to describe the wave pattern of mono-hulls for Froude numbers larger then 0.4-0.5, [1].
In the following the limits of application of this model to the trimaran will be shown.

4. DISCUSSION

As in [2] this section will be divided into two parts: 1) the description of the hull profiles and 2) of the wave pattern in the transom region.

4.1 Hull Profiles

In [2] a detailed comparison among numerical and experimental results has been carried out for Froude number from 0.4 to 0.7 with a rate $\Delta Fr = 0.1$.
Fig. 3 reproduces the comparison for the wave elevation along the main hull reported in that paper.
It shows that both the 2D+t and the 3D RPM solver are able to predict the wave elevation on the main hull for Fr = 0.4, but the 2D+t fails to predict the drop of the wave elevation behind the mid section of the ship both at Fr = 0.5 and 0.6. Instead, the 3D algorithm produces results closer to the experimental data.
At Fr = 0.7 things are reversed, the 2D+t gives a wave elevation closer to the one measured in the experiments, while the 3D solver predicts a too low wave profile all over the hull.

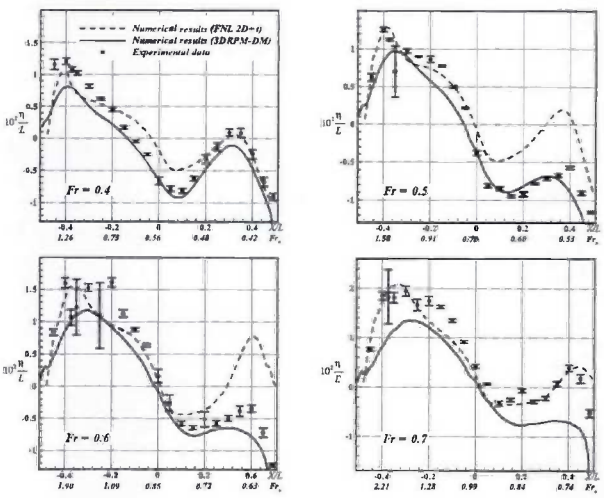

Fig. 3: *Wave profile along the main hull for four Fr numbers (indicated in each plot). Experiments (symbol: average value and error bar) and numerical data obtained by 3D-RPM (solid line) and 2D+t (dashed line). $Fr_x=U/(g\ x)^{0.5}$, with x the longitudinal distance from the bow. $L=L_{pp}$.Figure taken from [2].*

In Fig. 4, the analysis of contour lines of the steady wave pattern predicted by the 3D RPM (top of each plot) and the 2D+t (bottom) is reported similarly as in [2] but with the correct wave pattern for Fr = 0.5. The latter, in [2], was erroneously substituted with the one at Fr = 0.6.
The figure helps explaining the reason of the poor reliability of the second solver in the Froude range Fr= [0.5:0.6].
For increasing Froude numbers the lobes of the bow wave elongates. It is well known that the 2D+t, neglecting the longitudinal variation of the velocity, produces higher and longer bow waves. As a result of this, the wave generated by the main hull enters the regions between the latter and the outriggers at a lower Froude number than in reality. For example, at Fr = 0.5,

the bow wave is predicted to enter the region among the main and side hull by the 2D+t solver, while only the shoulder wave is interacting with the side hull according the 3D RPM solver. This limit plays an important role when different bodies are coupled together.

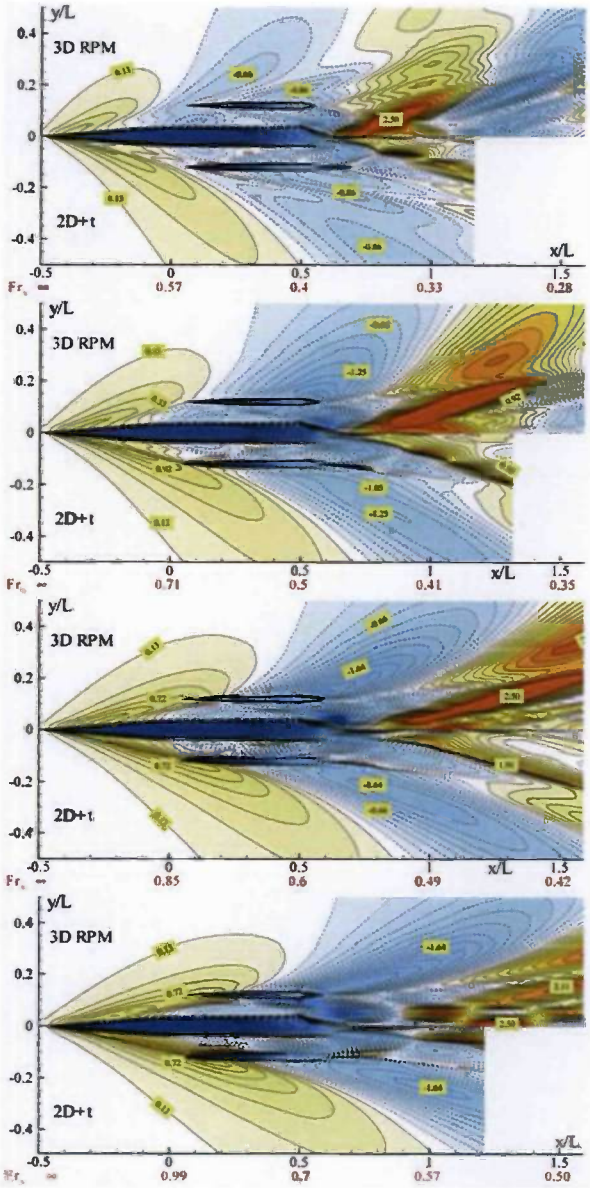

Fig. 4: *Contour lines of the steady wave pattern ($\eta/L \cdot 10^2$) as obtained by 3D-RPM (top) and 2D+t (bottom) numerical models for several Fr. From top to bottom: Fr=0.4, 0.5, 0.6, 0.7. $Fr_x=U/(g\ x)^{0.5}$, with x the longitudinal distance from the bow. $L=L_{pp}$. Figure taken from [2] except for results at Fr=0.5.*

In fact, the relative position of the wave systems can result in significant effect of interaction.

In the following, the wave field will be analyzed at Fr=0.5 and 0.7, to understand how much the solution of the 2D+t can be reliable at Fr≤0.7.

The lower value of the velocity has been chosen because it is the largest Fr at which the 2D+t fails to predict the wave pattern after the mid section. While the second one has been chosen because it is the smallest Froude number at which the 2D+t gives better results than 3D RPM solver with respect to the experiments.

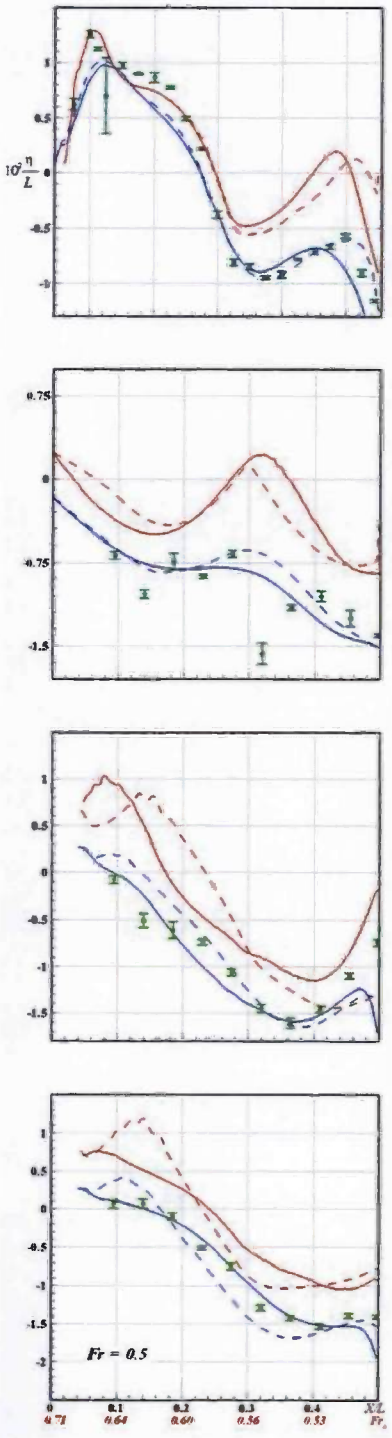

Fig. 5: *Fr = 0.5. From top to bottom: Wave profile along the main hull, along the central section among the hulls, along the internal side of the outrigger and along its external side. Symbols represent the experimental data; the solid red line is the 2D+t solution for the full trimaran; the solid blue line is the 3D RPM calculation and the dashed lines give the superposition of the wave fields obtained with the same solvers studying separately*

each hull. The colors for the latter are the same as the corresponding simulations for the full trimaran.

The aim here is to analyze the limits of the theoretical methods used, so that range of reliability can be stated. Moreover, we want to use the differences between the two algorithms to highlight the non linear effects developing in the interference region between the hulls.
To recover the effect of the linear and non-linear hydrodynamic interaction, the solution of the full trimaran configuration is compared with the linear superposition of the wave patterns generated by the single hulls (interference).
The comparison among the experimental data and the wave profiles calculated numerically at Fr= 0.5 is given in Fig. 5. The symbols represent the experimental data, the solid blue line stands for the 3D RPM solution, the solid red line for the results of the 2D+t calculations. The dashed lines refer to the wave profiles obtained by the same algorithms but applying the linear superposition of the flow fields generated by each single hull.
The repeatability analysis for the model tests is reported by presenting the experiments as average measured values and error bars. The latter are given as $\pm\sigma$, with σ the standard deviation.
For a correct evaluation of the limits of the 2D+t theory, the local Froude number Fr_x, defined with respect the local distance from the bow of the main hull, is also reported as secondary axis of the abscissas.
Numerically the wave elevation was calculated following the ship profile at a distance of 8mm from the hull to be consistent with the measurements.
As noted in [2], on the main hull (top plot of figure Fig. 5), both the 3D RPM and the 2D+t solver predict well the wave elevation in the front part. The non-linear solver is also able to capture the high deformation due to the jet-like flow at the bow. Somehow, the 3D solver smoothes the bow splash. This is partially due to a non-sufficient grid resolution. To describe more adequately the flow details, locally the mesh should be greatly refined for the 3D simulations.
In the fore region, small differences are noticeable between the solution for the full trimaran and the linear superposition, for the 3D RPM. While, due to the parabolic character (the upstream sections are not influenced by what happens downstream) there is no difference in the 2D+t data. The discrepancies appear after the mid section.
The causes of such differences can be fully understood only considering the effect of the side hull. The wave elevation on the internal and external part of the outrigger is shown in the 3rd and 4th plot of Fig. 5. There, even though the wave elevations predicted by the two solvers are different, the differences between the simulations accounting for (solid lines) or not accounting for (dashed lines) the interaction among the hulls are similar for the two solvers.
More in particular the difference in the wave height between the 2D+t and the 3D-RPM predictions, is almost constant and equal to the difference of wave height in the first section of the outrigger, i.e. $\Delta\eta$.

This difference can be explained through Fig. 6 showing the wave elevations as calculated by the two solvers for the mono-hull configuration in the transversal section coincident with the first section of the side-hull.
The linear solution is characterized by a lower wave height and by much less steep wave profile than the 2D+t data.

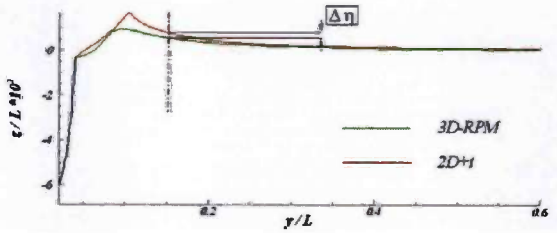

Fig. 6: *Fr = 0.5: transversal wave profile at the first section of the outrigger calculated by the 3D RPM and the 2D+t solvers for the mono-hull..*

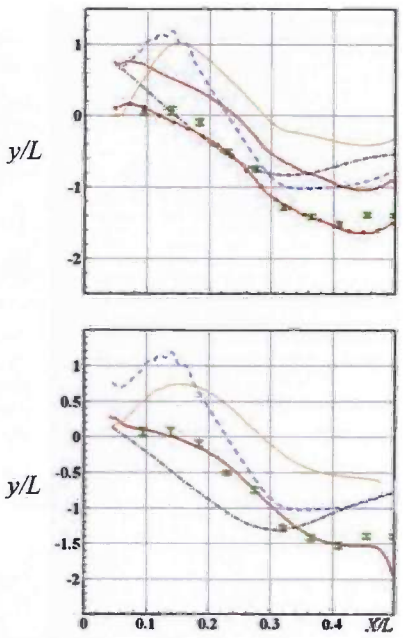

Fig. 7: *Fr 0.5: wave profiles along the external side of the outrigger calculated with the 2D+t solver (top figure) and the 3D RPM algorithm (bottom figure).Green symbols: experimental measurements; red solid line: full trimaran calculations; black dashed line: wave height on the side hull due to the only main hull; orange dotted line: wave profile along the side hull alone; blue dashed line: superposition of the main hull wave pattern to the ones due to the side hulls; solid red line with symbols: full trimaran results shifted by $\Delta\eta$.*

In the comparison with the experimental data both on the internal and on the external side of the side hull, the wave calculated by the 3D solver is closer to the experiments. Very likely, the steep wave generated by the main hull is smoothed in the linear calculation, in a way similar to the effect of the breaking.

Fig. 7 analyses also the effect of the shift $\Delta\eta$ on the external wave profile. Once shifted by $\Delta\eta$, the full trimaran results become very close to the experiments.
Moreover the figure shows the contribute of each single hull to the wave elevation. It can be noted that the hydrodynamic linear interaction is important on external part of the side hull: the side bow wave is significantly reduced and there is a drop of the water level in the back.
The wave elevation due to the only outrigger is equal in the internal and external region. Because the bow wave of the outrigger is cancelled in the full trimaran configuration of Fig. 5 predicted by 3D-RPM, we can deduce that there is a nullifying effect of the hydrodynamic interaction. Differently the 2D+t solution shows an evident first peak close to the bow. This is due to the reflection of the steep main bow wave, as already noted before. In the back, this interaction causes an increase of the water level.
Because these effects of interaction are similar in all the data collected along the outrigger, it can be deduced that the region close to the side hull is affected by a linear phenomenon of interaction.
The wave profiles on the main hull and in the mid section of Fig. 5 show that there the effects of interaction are almost null.

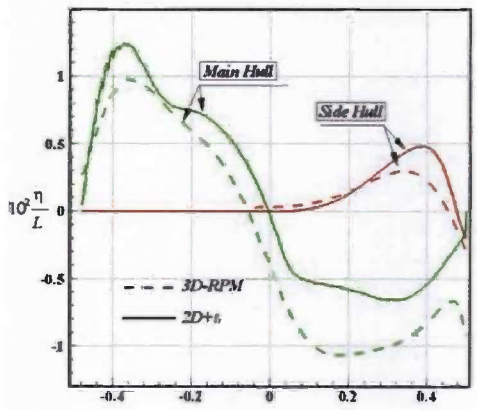

Fig. 8: *Cut of the waves generated by the isolated main and side hulls on the surface of the main hull*

The 2D+t is not able to capture properly the wave elevation close to the transom region of the main hull.
This is mainly due to the problems related to the wave elevation calculated in the main hull.
This part of the ship is the one that sees a lower Froude number, so that the 3D effects are not always negligible.
As shown in Fig. 8, where the absolute value of the wave trough in the aft part of the main hull calculated with the 2D+t solver is considerably lower than the one calculated with the 3D RPM algorithm.
Fig. 9 shows the wave profiles on the hulls at Fr = 0.7.
As in the previous case, the 2D+t algorithm results more accurate in reproducing the jet in the bow region of the main hull.
At this higher velocity, the lobes of the 2D+t are more similar to the one predicted by the 3D RPM and by the experiments, so that the reflection of the main bow wave on the outrigger is closer to the experiments.
Nonetheless the wave profile on the side hull calculated by the 2D+t for the full trimaran is higher than the one measured in the experiments and by the 3D solver.
Also in this case it is possible to calculate a $\Delta\eta$. However, the use of the shift does not explain the large region of discrepancies in the central section. More likely, a numerical error can be the cause of the difference. The more energetic wave induced by the cut of the jet, interacts for a longer period (and distance) with the outrigger. This increase of the water level in the front side of the outrigger can also play a role in the water drop in the region downstream.

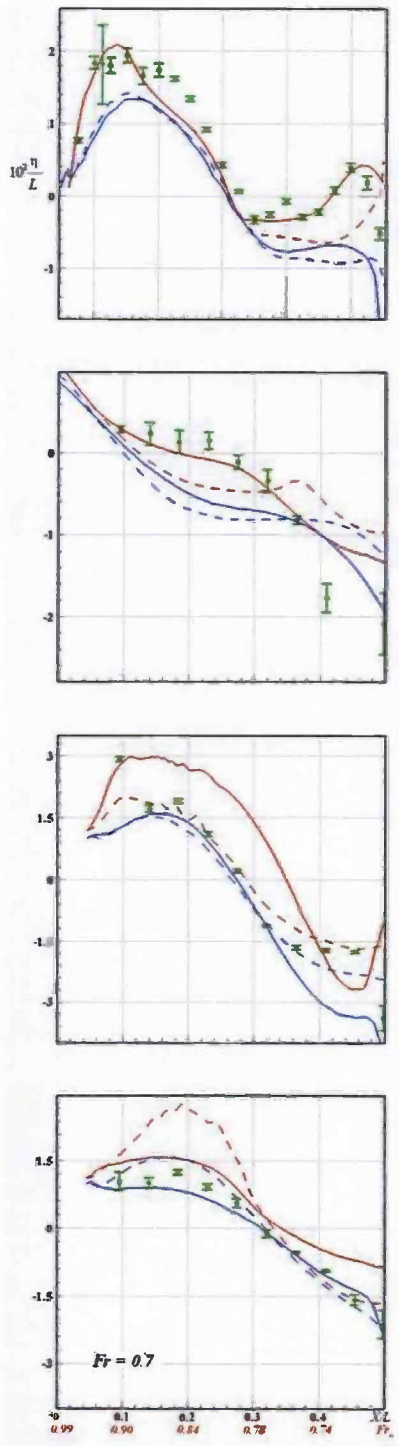

Fig. 9: *Fr = 0.7: From top to bottom: Wave profile along the main hull, along the central section among the hulls, along the internal side of the outrigger and along its external side. For the line legend* see Fig. 5.

Surprisingly the linear superposition seems closer to the experimental data than the full trimaran calculations.
No information for this matter can be obtained by the other solver. Both the linear superposition and the full trimaran 3D RPM calculations are very close to the experiments in the front side of the outrigger. The differences appear close to the transom, where the experiments result higher than both curves.
Some light can be shed on the effect of interference for the external profiles.

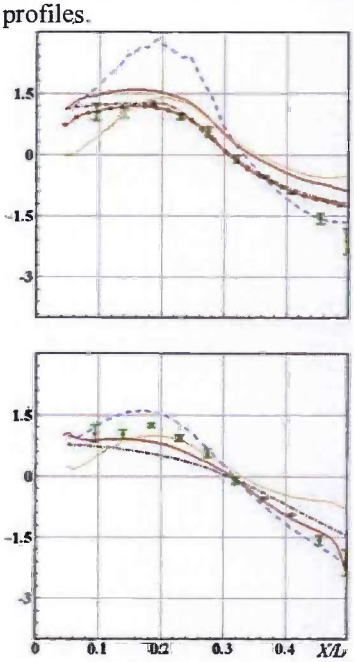

Fig. 10: *Fr 0.7, wave profiles along the external side of the outrigger calculated with the 2D+t solver (top figure) and the 3D RPM algorithm (bottom figure). For the line legend see Fig. 7.*

Fig. 10 gives the numerical wave profiles on the external side of the outrigger generated by the full trimaran calculations and by the linear superposition.
With the due shift the 2D+t full trimaran solution recovers the experimental data in the upstream region. Also the 3D RPM full trimaran solution is very close to the measured data, this means that in the external side the effects of hydrodynamic interaction are important and that they are linear. Even though the internal wave profile of the 2D+t solution does not resemble the measured data, the reflection of the wave in the internal region is well predicted as shown by the water height calculated in the central section and in the back of the main hull (see Fig. 9).
Analyzing the difference between the full trimaran and linear super-position solutions from the 2D+t theory and those from the 3D RPM solver for the mid-section (2nd plot from the top in Fig. 9), it is possible to deduce that the interaction between the outrigger bow wave and the reflection of the wave system by the main hull is non linear.
Only the nonlinear interaction can justify the higher wave height in the back of the main hull as well as in the central cut for x=[0.2,0.3]..
It is also interesting to note that the 2D+t solver shows errors in the wave height just before the transom region.
This is due to the assumption of a constant u along all the sections of the trimaran, the 3D RPM solver has been used to study the variation of velocity along the x.
It was expected that the region between the hulls was a region of acceleration of the flow, instead, as shown in Fig. 11, the variation of the horizontal velocity in the 3D RPM solution is smaller than the 8%. The largest variations of the velocity are localized at the stagnation point in the front of the hulls and close to the transom region where the differences between the 2D+t solution and the experiments appear more evident.

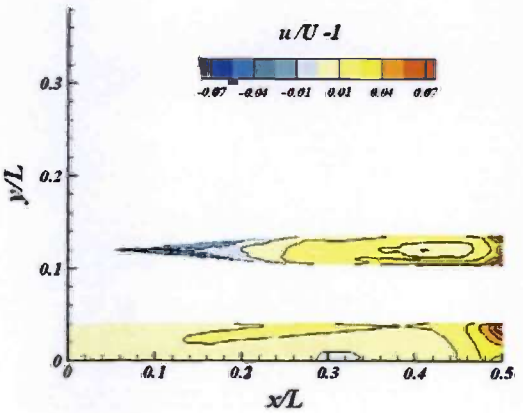

Fig. 11: *Variation of the horizontal velocity along the trimaran hulls calculated with the 3D RPM algorithm.*

4.2 Steady case: Transom Flow

Fig. 12 shows the comparison between the wave patterns behind the stern calculated numerically with the 2D+t and with the 3D RPM solvers. The two solutions given for each method represent, respectively, the simulation for the full trimaran configuration and the solution obtained superimposing the wave patterns generated by each single hull. The Froude number considered is Fr=0.5.
The drawback of an elongated wave pattern for the 2D+t solution is evident behind the transom region. There, the three-dimensional effects are more important: a deceleration of the flow occurs just behind it. In [1], the differences between the numerical results and the experimental data have already been analyzed for the mono-hull, showing that the solver can be considered reliable only for very high Froude numbers and not immediately behind the transom.
In the case of the trimaran, the 3D region is as wide as the trimaran. This implies that the wave pattern obtained

with the 2D+t algorithm is to be used only qualitatively to understand the deformation of the wave system.
The comparison among the two numerical solutions and the experimental measurements shows that the wave elevation calculated by the 3D RPM solver is higher than the ones predicted by the 2D+t solver and measured in the tank.

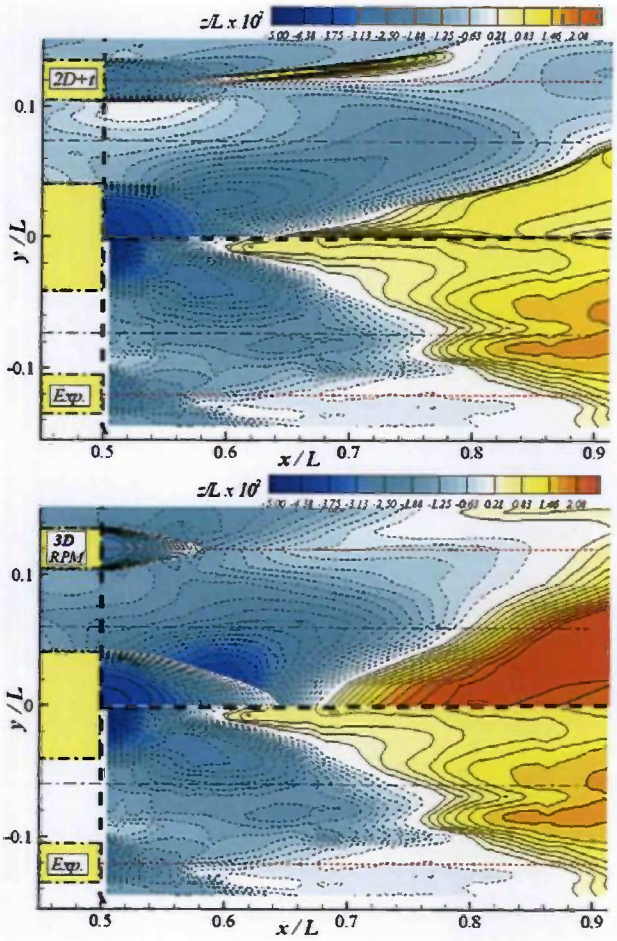

Fig. 12: *Fr = 0.5 comparisons of the wave fields behind the transom stern.*

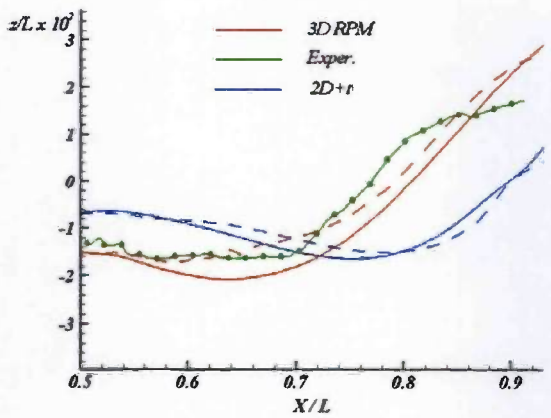

Fig. 13: *Fr = 0.5: wave height at y/L=0.0737; the solid lines represent the wave elevation for the full trimaran, the dashed lines of the same colour the linear superposition obtained with the same solver.*

To study the cause of this difference, Fig. 13 shows the cut of the wave along the line in the centre of the main and side hull. In the figure the wave height generated by summing the wave elevations generated in that section by each single hull is plotted with a dashed line.
The wave field generated by the side hull is affected by the linear interaction among the wave systems that causes the wave to be deviated sideways as shown by each data set reported in the figure.

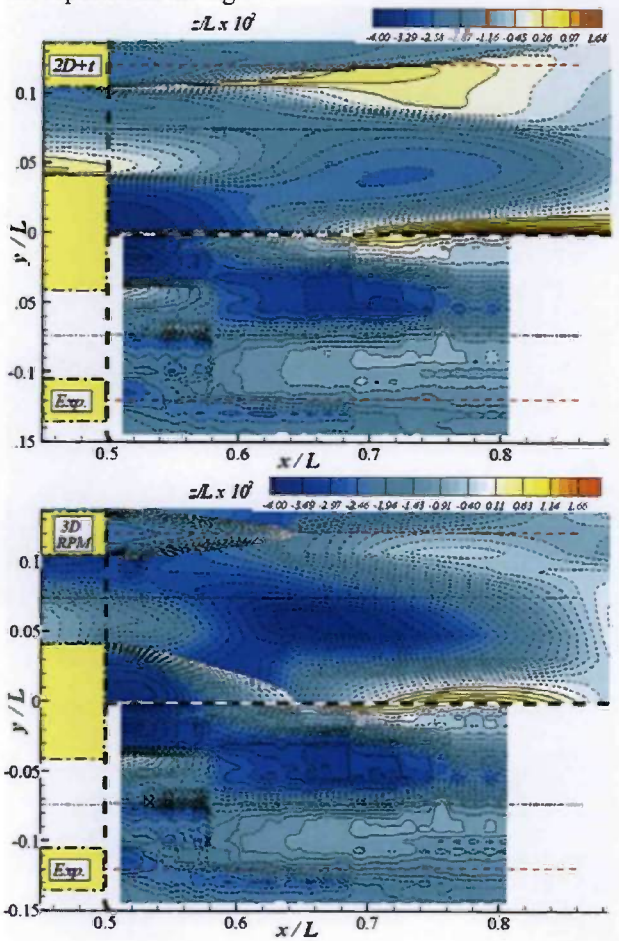

Fig. 14: *Fr = 0.7: comparisons of the wave fields behind the transom stern.*

Fig. 14 shows the wave pattern behind the transom at Fr=0.7. Due to the higher Fr, the wave system generated at the transom is elongated downstream, so that the rooster tail is not completely visible in the picture. The solution of the 2D+t presents a higher wave elevation and an expected shift downstream of the wave system; the 3D RPM presents a shift too, even though reduced with respect to the other solver.
This difference could be due to the shape adopted for the false body. So a new shape has been introduced for the central hull; it is obtained using the experimental data for the second curve described in section 3.1. Fig. 15 shows the wave elevation obtained with the new shape. The trough at y=0.05 and the crest in the mid section results closer to experimental data. The main problem with this

curve is the reconnection with the transom section of the hull.
In the future we plan to adopt the curve described by Faltinsen in [10]; with an iterative algorithm based on the assumption of null pressure at the transom, we want to determine the coefficients of such curve.

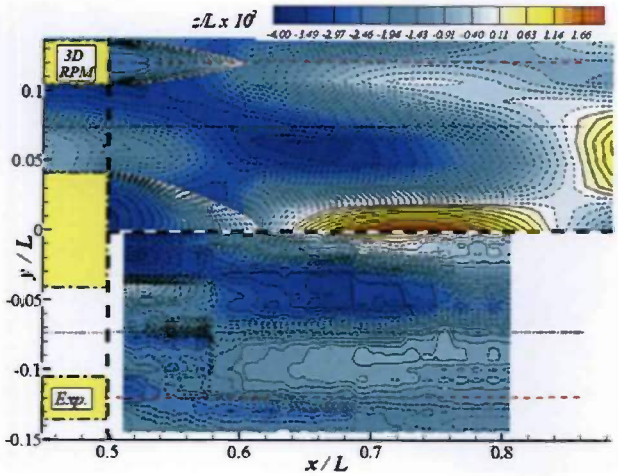

Fig. 15: *Fr = 0.7: wave profile behind a transom stern modelled with a 3D RPM solve. The false body is obtained using the experimental data.*

Another possible solution is the use of an iterative method that models the 3D shape of the hull hollow assuming that the pressure on it has to be zero. Something similar has been presented in [11] with the modified flexible appendage model.
The cuts of the wave pattern at y/L=0.05 and 0.1 are reported in Fig. 16. The 3D RPM solver is able to capture the decrease of the water level in this section, so that the results are very close to the experimental data. The water level results even closer to experiments if the experimental wave elevation is used to model the false body along the x axis (black line with symbols in Fig. 16). As expected, the same drop is predicted by the 2D+t solver but further downstream.

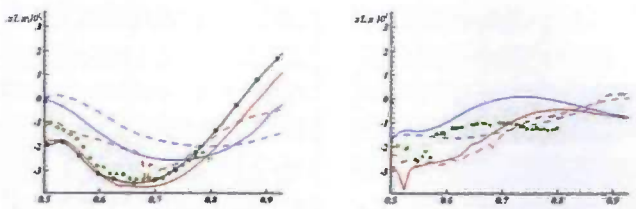

Fig. 16: *Fr = 0.7: wave height at y/L = 0.05 (left plot) and y/L = 0.1 (right plot); the solid lines represent the wave elevation for the full trimaran, the dashed lines of the same colour the linear superposition obtained with the same solver. In the left plot the black line with symbols represents the wave elevation obtained by the 3D RPM solver using the experimental data to model the false body.*

The cut closer to the side hulls intersects the crest created in the wave of the outrigger. This wave is strongly influenced by the interference among the different wave systems, so that the 2D+t solution affected by 3D errors of different intensity on the main and side hull gives a completely different solution. The wave cut of the 3D RPM solution shows a magnitude similar to the experiments but, as stressed above, the shift downstream of the wave system causes the 3D RPM solver to present the maximum of the wave height in a later section. For the side hull it was not possible to use the experimental data to model the false body, because it was not possible to find an analytical reconnecting curve among the experiments in the mid section of the outrigger and transom section. This implies that a careful study of the false body is necessary to recover the wave elevation in the transom region. This is going to be the aim of the future work.

CONCLUSIONS

A comprehensive experimental and numerical investigation has been carried out to study the steady flow field around a trimaran vessel. The validity of the fully nonlinear 2D+t theory and a 3D-RPM numerical models has been investigated.
The 2D+t range of reliability has been stated. While for a monohull it can be considered reliable from Fr > 0.5, for multihull configurations it is able to capture both the interference and the interaction effects among the hulls from Fr ≥ 0.7.
Close to the transom and behind it the 3D effects become very important and the 2D+t solver is not able to capture the wave profile correctly.
The numerical tools have been used to identify the regime of interaction among the wave fields generated by each single hull.
The region close to the main hull is characterized by small effects of interaction at low Froude numbers.
With the velocity increasing, the interaction becomes more important and nonlinear. The latter occurs at Fr = 0.7.
This implies that the 3D RPM algorithm starts to lack reliability.
For the transom region, because of the 3D effects, it has been confirmed that the 2D+t solver is able to give only a qualitative representation of the wave field. Instead the 3D RPM solver is able to predict the wave pattern in an almost satisfactory way, even though its limit of being a linear solver is evident.
Moreover the analysis of the results at the higher velocity has highlighted the need of a proper description of the false body behind the transom stern.

ACKNOWLEDGMENTS

Present research activity is partially supported by the Centre for Ships and Ocean Structures, NTNU, Trondheim, within the "GreenWater Events and Related Structural Loads" project, and partially done within the framework of the "Programma di Ricerca sulla Sicurezza" funded by *Ministero Infrastrutture e Trasporti*.

REFERENCES

[1] LUGNI C., COLAGROSSI A., LANDRINI M., FALTINSEN O.M., 'Experimental and numerical study of semi-displacement mono-hull and catamaran in calm water and incident waves', St. John's, Proc. 25th Symp on Naval Hydrod., pp. 104-119, 2004.

[2] COLICCHIO, G., COLAGROSSI, A., LUGNI, C., FALTINSEN, O.M., 'Experimental and numerical investigation of a Trimaran in calm water', Proceeding of the International Conference on Fast Sea Transportation, 2005.

[3] SAHOO, P.K., DOCTORS, L.J. 'The Waves Generated By a Trimaran', Proceeding of the International Conference on Fast Sea Transportation, 2005.

[4] ZHAO, R. , O. M. FALTINSEN. 'Water entry of two dimensional bodies' J. Fluid Mech. Vol. 243, pp. 593–612, 1993.

[5] NAKOS, D.E., 'Ship Wave Patterns and Motions by a Three Dimensional Rankine Panel Method', MIT, Cambridge, 1990.

[6] HESS J.L., SMITH A.M.O.,'Calculation of non--lifting potential flow about arbitrary bodies', Prog. Aero. Sci., vol. 8, 1-138, 1996.

[7] BERTRAM V., 'Fulfilling Open-Boundary and Radiation Condition in Free-Surface Problems Using Rankine Sources', Ship Technology Research, vol. 37,1990.

[8] DOCTORS, L.,' Hydrodynamics of the flow behind a transom stern'. Proceedings of 29th Israel Conference on Mechanical Engineering, pp. 1–11. Haifa, Israel, 2003.

[9] RAVEN H.C.,'A solution Method for the Nonlinear Ship Wave Resistance Problem', PhD thesis, University of Delft, The Netherlands, 1996.

[10] FALTINSEN, O.M.,' Hydrodynamics of high speed marine vehicles', Cambridge Univ. Press, 2005.

[11] AHMED, T.M., DU, S.X., HUDSON, D.A., KINGSLAND P.W., TEMAREL P., 'Improvement of seakeeping prediction methods for high speed vessels with a transom stern', Proceeding of the International Conference on Fast Sea Transportation, 2005.